Low anisotropic upper critical fields in $SmO_{1-x}F_xFeAs$ thin films with a layered hybrid structure

Silvia Haindl[1,*], Erik Kampert[2], Masato Sasase[3], Hidenori Hiramatsu[3,4], Hideo Hosono[3,4]

[1] World Research Hub Initiative (WRHI), Institute of Innovative Research, Tokyo Institute of Technology, 4259 Nagatsuta-cho, Midori-ku, Yokohama, Kanagawa 226-8503, Japan

[2] Dresden High Magnetic Field Laboratory (HLD-EMFL), Helmholtz-Zentrum Dresden-Rossendorf, 01328 Dresden, Germany

[3] Materials Research Center for Element Strategy, Tokyo Institute of Technology, Mailbox SE-1, 4259 Nagatsuta-cho, Midori-ku, Yokohama, Kanagawa 226-8503, Japan

[4] Laboratory for Materials and Structures, Institute of Innovative Research, Tokyo Institute of Technology, Mailbox R3-3, 4259 Nagatsuta-cho, Midori-ku,Yokohama, Kanagawa 226-8503, Japan

* corresponding author's email address: haindl.s.aa@m.titech.ac.jp

Abstract

We report on the upper critical fields in $SmO_{1-x}F_xFeAs$ thin films prepared by pulsed laser deposition. With an F-content gradient along their thickness, the films could be described approximately as layered two-phase hybrid structures comprised of one superconducting layer and one antiferromagnetic layer. An analytical characterization of different thin film samples by AES and STEM-EDX is provided and structural defects, such as antiphase boundaries, were confirmed for films grown at lower deposition temperatures. Electrical transport measurements in pulsed magnetic fields yielded upper critical fields higher than 80 T with an anisotropy $\gamma_{Hc2} \leq 2.25$.

Introduction

Among the iron-pnictides, the iron-oxypnictides of composition (*RE*)FeAsO (*RE* = rare earth) reach the highest critical temperatures, T_c, and upper critical fields, $\mu_0 H_{c2}$, upon substitution of oxygen (O) by fluorine (F) [1]. Since their discovery in 2008 a stepwise progress in the synthesis of thin films has been made. At present, epitaxial iron-oxypnictide thin films can be grown using *i)* molecular beam epitaxy (MBE) [2 – 4], *ii) ex-situ* heat treatment after pulsed laser deposition (PLD) at room-temperature (two-step method) [5, 6], and, *iii)* by *in-situ* PLD [7 – 10]. The latter method, an *all in-situ* PLD process, has been an underdeveloped subject since 2016. For each synthesis method the incorporation of fluorine – and hence the control of electron doping – poses enormous challenges as well as the reduction of impurity phase formation. Moreover, the interpretation of physical quantities requires detailed information of the composition and microstructure of the films [11].

Here we report on the upper critical fields of $SmO_{1-x}F_xFeAs$ thin films grown on CaF_2 substrates by *in-situ* PLD. The films become superconducting due to F-diffusion from the substrate into the SmOFeAs-phase activated by the high substrate temperatures of ~860°C during film growth. The obvious advantage of the diffusion process is the substitution of O by F resulting in a superconducting $SmO_{1-x}F_xFeAs$ phase. However, the presence of an F-diffusion gradient along the film thickness challenges the growth of homogeneous films. The inevitable interdiffusion at the film/substrate (F/S) interface including the diffusion of oxygen from the film into the substrate may lead to a natural passivation of the interface, which has not been considered previously.

In addition to the determination of the upper critical fields we present a qualitative analysis of the chemical composition of the PLD-grown films by Auger electron spectroscopy (AES) and combined depth profiling as well as by energy-dispersive X-ray spectroscopy in scanning transmission electron microscopy (STEM-EDX). Since the electronic ground state of $SmO_{1-x}F_xFeAs$ depends on the F-content, x, [12, 13] an F-diffusion gradient along the film thickness spatially confines superconductivity to a layer close to the F/S interface where $x \geq 0.1$, whereas a second layer up to the film surface is dominated by the antiferromagnetic phase with $x \rightarrow 0$. Hence, the films grown by PLD can be modeled in a first approximation as layered two-phase hybrid

structures with a thinner F-rich (superconducting) layer and a thicker F-poor (antiferromagnetic) layer on top of it (Fig. 1).

Experimental

$SmO_{1-x}F_xFeAs$ thin films were grown by PLD (base pressure of the ultra-high vacuum chamber is about $6 \cdot 10^{-8}$ mbar) using a Nd:YAG(2ω) laser (λ = 532 nm) with a repetition rate of 10 Hz and a non-doped SmOFeAs target. Film growth rates were approximately 1 $Å s^{-1}$. Films were grown epitaxially with *c*-axis lattice parameters slightly larger than those in comparable bulk samples. The *c*-axis lattice parameters were determined by X-ray diffraction (in Bragg Brentano geometry) using a Rigaku Smart Lab diffractometer (Cu Kα). Film thicknesses were measured by X-ray reflectivity analysis and by scanning transmission electron microscopy (STEM). Details of the thin film preparation and characterization can be found in Ref. [8].

CaF_2(001) substrates were heated to 860°C for the deposition of $SmO_{1-x}F_xFeAs$ thin films (films nos. 2,3). F-diffusion was previously reported at around 800°C, for example, for an $YBa_2Cu_3O_{7-\delta}$ film grown on CaF_2 [14] and also from a CaF_2 cover layer into a NdOFeAs film [15]. Additionally, the alkaline earth metal difluorides are known to exhibit ionic conductivity at elevated temperatures due to the mobility of fluorine interstitials and fluorine vacancies [16]. Moreover, the lattice constant of CaF_2(001), or technically speaking, the atomic distance at the surface ($a/\sqrt{2}$ = 3.863 Å) adapts to the *a*-axis lattice parameter of the iron-oxypnictides. Misfit dislocations are easily formed for larger lattice mismatches. In summary, CaF_2(001) substrates facilitate epitaxial film growth and simultaneously act as doping source during synthesis.

F-diffusion from the CaF_2(001) substrate into the growing SmOFeAs phase has also been observed in MBE film growth, however due to the lower substrate temperature of 650°C the resulting films were underdoped and an F-containing capping layer was added in order to increase the F-content in the films [17]. For comparison, we also have grown a film at this reduced temperature (film no. 1) but no superconducting transition was observed. The properties of the thin film samples investigated here are summarized in Table 1. The F-content is mainly regulated by temperature and the deposition time which corresponds approximately with the duration of F-diffusion from the substrate into the film.

Auger electron spectroscopy (AES) was carried out using an ULVAC-Phi 710 Auger electron spectrometer with an integrated scanning electron microscope and an Ar sputtering gun for depth profile analysis. The elemental analysis was performed with a 10 kV primary energy, an electron current of 5 nA on an area of 200 µm in diameter that resulted in a current density of around 3.77 µA/cm^2 (corresponding to an electron density of $7.6 \cdot 10^{17}$ e$^-$/cm^2). The choice of the parameters was according to an observed induced F-diffusion during depth profiling for higher electron densities of $5.5 \cdot 10^{18}$ e$^-$/cm^2 (Appendix). For the depth profile full spectra (from E_{kin} = 30 eV to 1300 eV) were recorded every 2 minutes. Spectra in selected energy ranges (including low energy transitions of Sm, O KLL, Fe LMM, F KLL and As LMM transitions) were recorded in steps of 30 seconds.

High-angle annular dark-field scanning transmission electron microscopy (HAADF-STEM) and energy-dispersive X-ray spectroscopy (EDX) were carried out in a JEOL JEM-ARM 200F operating at 200 kV. TEM specimens were prepared by ion milling and a focused ion beam (FIB) using a JEOL JIB-4610F system. The EDX mapping range was 0 – 20 keV with an acquisition time of 5 minutes.

Electrical transport measurements (four point method) for films nos. 2,3 were carried out at the Dresden High Magnetic Field Laboratory in pulsed magnetic fields up to 62 T, with a pulse duration of about 150 ms, both parallel and perpendicular to the *c*-axis of the films. The dimensions of the films for the transport measurements were 70 mm × 30 mm × 58 nm (film no. 2) and 50 mm × 20 mm × 91 nm (film no. 3). AC currents of 100 µA and frequencies of 16 – 25 kHz were applied to the films, and the voltages were recorded using a 1 MS/s 16-bit Yokogawa DL750 oscilloscope. The resistances of the films were calculated by applying a digital lock-in procedure to the recorded data. For the electrical contacts a conventional silver paste was used. The temperature was controlled using a liquid ^{4}He bath cryostat and a local heater near the films, which were placed inside a stainless steel jacket with a He atmosphere. In order to confirm temperature stability during the magnetic field pulses, the resistance of a Cernox thermometer near the films was additionally recorded. Complementary, for selected films the electrical resistance was measured in static magnetic fields up to 14 T using a conventional physical properties measurement system (PPMS).

Results and Discussion

The $SmO_{1-x}F_xFeAs$ thin films were analyzed by AES and STEM-EDX. Fluorine is detected within the films (films nos. 2,3) near the F/S interface and its concentration is gradually reducing with increasing distance from the substrate. From AES depth profiling the intensity of the F $KL_{2,3}L_{2,3}$ transition could be traced up to approximately 10 nm into the thin film before it overlapped with the background of the Fe $L_{2,3}M_{2,3}M_{4,5}$ transition at ~650 eV. This value may serve as a minimum estimate of the effective thickness of the superconducting layer. The F-gradient along the film thickness was confirmed by EDX/TEM mapping (Fig. 2). Accordingly, the resistive transitions from the normal to the superconducting state showed the typical broadening as already reported in Ref. [8].

Both AES and STEM-EDX revealed a narrow Ca-diffusion zone close to the F/S interface and a decreased Fe concentration at the surface of the film. Furthermore, STEM-EDX also indicated a small amount of counter-diffusion of Sm-, Fe- and O from the film into the substrate (Fig. 2). O-diffusion into CaF_2 can lead to a passivation of the interface resulting in a progressing reduction of F-diffusion into the film with time. For the investigated films deposited at 860°C with deposition times of 10 min (thickness ≈ 60 nm) and 15 min (thickness ≈ 90 nm) such a possible passivation effect was not observed. With longer F-diffusion at 860°C an increase in $T_c(0)$ by ~10 K was observed. The HAADF-STEM results indicated that the F/S interface is sometimes less abrupt for films grown at high temperatures and the substrate lattice contains a lot of dislocations. This is certainly the effect of the high temperature on the CaF_2 lattice during deposition. However, also regions with abrupt F/S interface could be found indicating a lateral inhomogeneity.

The layered structure of the oxypnictide films was observed by HAADF-STEM. Due to the Z-contrast lattice planes of Sm atoms are visible best. The analysis also revealed the occurrence of stacking faults and antiphase-boundaries (APBs) [18] parallel to the *c*-axis with a displacement vector of $c/2[0, 0, 1]$ in the film grown at a lower temperature (film no 1). The presence of ABPs in films grown at 860°C is less clear. The growth of the SmOFeAs unit cell on $CaF_2(001)$ may have either started with the FeAs or the SmO layer. The APBs occur with grain coalescence and can heal out after the introduction of further stacking faults. The presence of APBs in the initial growth of iron-oxypnictide thin films might inhibit superconductivity and, therefore, suppress critical

current densities, because the superconducting FeAs planes are disrupted. At the present stage the density of these defects and their quantitative effect on electrical transport properties are unknown. Qualitatively, the APBs could explain the often observed negative temperature coefficient, dR(T)/dT, of the resistance of iron-oxypnictide thin films.

Pulsed magnetic field measurements resulted in gradual normal-to-superconducting transitions. The magnetoresistance of the normal phase (above T_c) was small and for $\mu_0 H \parallel ab$ nearly constant (Fig. 4). The strong broadening of the transitions could be attributed to the F-content gradient in the films.

The slopes, dH_{c2}/dT, do not show a strong saturation tendency at the highest magnetic fields accessible for our measurement. An extrapolation of the upper critical fields down to 0 K indicates values of $\mu_0 H_{c2}(0)$ higher than 80 T (Fig. 5). The corresponding Ginzburg-Landau coherence length, $\xi_{ab}(0)$, was smaller than 2 nm. The upward curvature and the absence of a saturation tendency was observed for $\mu_0 H \parallel c$ down to temperatures of 1.9 K. This observation is similar to a $LaO_{1-x}F_xFeAs$ and $(La_{1-y}Sm_y)O_{1-x}F_xFeAs$ thin films synthesized by a two-step method based on an *ex-situ* heat treatment [19, 20]. Such a temperature dependence of the upper critical field is reflected in the temperature dependence of the $\mu_0 H_{c2}$-anisotropy at low temperatures. In iron oxypnictides the $\mu_0 H_{c2}$-anisotropy, defined as $\gamma = H_{c2\parallel ab}/H_{c2\parallel c}$, typically takes values between 2 and 5 and decreases moderately with decreasing temperature. The initial steep slopes for dH_{c2}/dT near T_c result in very large and overestimated γ-values. For $T \rightarrow 0$ the upper critical field tends to become more isotropic. Evaluated for the 75% criterion the layered hybrid structures reached small γ-values below 2.25 (at ~15 K for film no. 2 and at ~28 K for film no. 3) that are decreased even further with decreasing temperature (Fig. 5 inset).

The actual temperature variation of the upper critical fields (data points in Fig. 5) may contain also changes in the curvature that arise from the multiband nature of the superconductors or from the proximity of the antiferromagnetic part of the hybrid structure that are not captured by the interpolated line (red line in Fig. 5). At present we can only estimate the antiferromagnetism of the upper film layers by the decreased F-content. The large T_c and H_{c2} values and the confined accessible range of the $H_{c2}(T)$-diagram as well as the number of unknown parameters in the

modelling of $H_{c2}(T)$ make a precise fit difficult. Further experiments would be necessary for a complete understanding of $\mu_0 H_{c2}(T)$.

Taking the 10%-criterion as an upper estimation of the irreversibility line, the $\mu_0 H(T)$-phase diagram also indicated a large reversible (flux flow) regime (between blue and red data points). Finally, from a comparison with the available T_c and $H_{c2}(T)$ curves for $SmO_{1-x}F_xFeAs$ crystals we estimated the F-content of the superconducting films to be $0.1 \leq x \leq 0.12$ and $0.12 \leq x \leq 0.15$, respectively [21, 22].

Conclusions

$SmO_{1-x}F_xFeAs$ thin films prepared on CaF_2 substrates at 860°C by *in-situ* PLD were characterized by interdiffusion through the F/S interface. Whereas lattice defects such as APBs could be detected in the initial film growth at lower deposition temperatures, doping by F-diffusion became effective only at higher temperatures. The F-content increases with the duration of the activated diffusion process during deposition. The F-content gradient divided the films into two layers: a thin superconducting layer (with x around 0.10 – 0.15) near the F/S interface and an non-superconducting and antiferromagnetic layer (with $x \rightarrow 0$) on top. The effective thickness of the superconducting layer in the investigated films was estimated to be in the range of 10 – 15 nm. The thin $SmO_{1-x}F_xFeAs$ layers stayed superconducting even in very high magnetic fields despite the proximity of an antiferromagnetic phase (layer). The $\mu_0 H_{c2}$-anisotropy of the layered hybrid structures was below 2.25 (for $T < 0.6\ T_c$) and might decrease further at lower temperatures.

Appendix

Note on the interaction of CaF_2 substrates with electron beams:

CaF_2 crystals severely interact with electron beams, which may cause limitations in the analytical investigation (based on electron probes) of films grown on these substrates. For example, during AES an sudden strong increase of the F-content arises in the depth profile when an electron density of around $5.5 \cdot 10^{18}$ e^-/cm^2 is used. Furthermore, the bare substrate surface strongly charged up.

A too strong focusing of the electron beam before EDX mapping may also have induced a small F-signal found in film no. 1 by STEM-EDX mapping (Fig. A1). Since the deposition temperature of film no. 1 is lower than 860°C no strong interdiffusion occured compared to film no. 2 (Fig. 2) and the F/S interface seems to be also abrupt (location indicated by an arrow). As indicated in the text, APBs found in film no. 1 might also inhibit the superconducting pairing mechanism.

Thin film characterization by XRD:

Fig. A2 summarizes the X-ray diffractograms ($2\theta/\omega$) for the discussed thin film samples. We have indicated the 00l reflections of the $Sm(O_{1-x}F_x)FeAs$ phase only once as well as the Fe 110 reflection of the impurity phase (*). In sample no. 1 a very small peak found near $2\theta/\omega = 26°$ can be indexed as SmAs 111 reflection (o). The corresponding SmAs 222 reflection is hidden by the $Sm(O_{1-x}F_x)FeAs$ 005 reflection. Fe and SmAs are typical impurity phases in $Sm(O_{1-x}F_x)FeAs$ thin films grown by PLD.

References

[1] R. Wesche: Physical Properties of High-Temperature Superconductors. Wiley Series in Materials for Electronic & Optoelectronic Applications. John Wiley & Sons, Ltd. (2015) pp 473-475

[2] T. Kawaguchi, H. Uemura, T. Ohno, R. Watanabe, M. Tabuchi, T. Ujihara, K. Takenaka, Y. Takeda, H. Ikuta: Epitaxial growth of NdFeAsO thin films by molecular beam epitaxy. Appl. Phys. Express 2, 093002 (2009)

[3] S. Ueda, S. Takeda, S. Takano, A. Yamamoto, M. Naito: High-Tc and high-Jc SmFeAs(O,F) films on fluoride substrates grown by molecular beam epitaxy. Appl. Phys. Lett. 99, 232505 (2011)

[4] H. Sugawara, T. Tsuneki, D. Watanabe, A. Yamamoto, M. Sakoda, M. Naito: One-step growth of SmFeAs(O,F) films by molecular beam epitaxy using FeF_2 as a fluorine source. Supercond. Sci. Technol. 28, 015005 (2015)

[5] E. Backen, S. Haindl, T. Niemeier, R. Hühne, T. Freudenberg, J. Werner, G. Behr, L. Schultz, B. Holzapfel: Growth and anisotropy of La(O,F)FeAs thin films deposited by pulsed laser deposition. Supercond. Sci. Technol. 21, 122001 (2008)

[6] S. Haindl, M. Kidszun, F. Onken, A. Mietke, T. Thersleff: Lessons from oxypnictide thin films. Int. J. Mod. Phys. B 27, 1330001 (2013)

[7] H. Hiramatsu, T. Katase, T. Kamiya, M. Hirano, H. Hosono: Heteroepitaxial growth and optoelectronic properties of layered iron oxyarsenide, LaFeAsO. Appl. Phys. Lett. 93, 162504 (2008)

[8] S. Haindl, K. Hanzawa, H. Sato, H. Hiramatsu, H. Hosono: *In-situ* growth of superconducting $SmO_{1-x}F_xFeAs$ thin films by pulsed laser deposition. Sci. Rep. 6, 35797 (2016)

[9] S. Haindl, S. Molatta, H. Hiramatsu, H. Hosono: Recent progress in pulsed laser deposition of iron based superconductors. J. Phys. D: Appl. Phys. 49, 345301 (2016)

[10] S. Haindl, H. Kinjo, K. Hanzawa, H. Hiramatsu, H. Hosono: Pulsed laser deposition of $SmFeAsO_{1-\delta}$ on MgO(100) substrates. Appl. Surf. Sci. 437, 418 (2018)

[11] S. Haindl, M. Kidszun, S. Oswald, C. Hess, B. Büchner, S. Kölling, L. Wilde, T. Thersleff, V. V. Yurchenko, M. Jourdan, H. Hiramatsu, H. Hosono: Thin film growth of Fe-based superconductors: from fundamental properties to functional devices. A comparative review. Rep. Prog. Phys. 77, 046502 (2014)

[12] R. H. Liu *et al.*: Anomalous transport properties and phase diagram of the FeAs-based $SmFeAsO_{1-x}F_x$ superconductors. Phys. Rev. Lett. 101, 087001 (2008)

[13] A. J. Drew *et al.*: Coexistence of static magnetism and superconductivity in $SmFeAsO_{1-x}F_x$ as revealed by muon spin rotation. Nat. Mater. 8, 310 (2009)

[14] R. P. Vazquez, M. C. Foote, B. D. Hunt, J. B. Barner: Growth of $YBa_2Cu_3O_{7-\delta}$ on alkaline earth fluoride substrates and thin films. Physica C 207, 266 (1993)

[15] N. Sumiya, T. Kawaguchi, M. Chihara, M. Tabuchi, T. Ujihara, A. Ichinose, I. Tsukada, H. Ikuta: Growth of a smooth CaF_2 layer on NdFeAsO thin film. J. Phys.: Conf. Ser. 507, 012047 (2014)

[16] R. W. Ure: Ionic Conductivity of Calcium Fluoride Crystals. J. Chem. Phys. 26, 1363 (1957)

[17] S. Takeda, S. Ueda, S. Takano, A. Yamamoto, M. Naito: Growth of superconducting SmFeAs(O,F) epitaxial films by F diffusion. Supercond. Sci. Technol. 25, 035007 (2012)

[18] R. J. D. Tilley: Defects in Solids. Wiley (2008) p.114-116

[19] M. Kidszun. S. Haindl, T. Thersleff, J. Hänisch, A. Kauffmann, K. Iida, J. Freudenberger, L. Schultz, B. Holzapfel: Critical current scaling and anisotropy in oxypnictide superconductors. Phys. Rev. Lett. 106, 137001 (2011)

[20] S. Haindl, M. Kidszun, E. Kampert: Iron pnictide thin films: Synthesis and physics. Phys. Stat. Sol. B 254, 1600341 (2017)

[21] H.-S. Lee, M. Bartkowiak, J.-H. Park, J.-Y. Lee, J.-Y. Kim, N.-H. Sung, B. K. Cho, C.-U. Jung, J. S. Kim, H.-J. Lee: Effects of two gaps and paramagnetic pair breaking on the upper critical field of $SmFeAsO_{0.85}$ and $SmFeAsO_{0.8}F_{0.2}$ single crystals. Phys. Rev. B 80, 144512 (2009)

[22] C. Senatore, R. Flükiger, M. Cantoni, G. Wu, R. H. Liu, X. H. Chen: Upper critical fields well above 100 T for the superconductor $SmFeAsO_{0.85}F_{0.15}$ with T_c = 46 K. Phys. Rev. B 78, 054514 (2009)

Acknowledgments

All authors thank Michiko Sato for performing AES measurements and Masaki Ichihara for assisting in TEM specimen fabrication and STEM-EDX measurements. All authors also acknowledge the support of the HLD-HZDR, a member of the European Magnetic Field Laboratory (EMFL). H. Ho., H. Hi., and M. S. are supported by the Ministry of Education, Culture, Sports, Science, and Technology (MEXT) through the Element Strategy Initiative to Form Core Research Center. H. Hi. was also supported by the Japan Society for the Promotion of Science (JSPS) through Grants-in-Aid for Scientific Research (A) and (B) (Grant Nos. 17H01318 and 18H01700), and Support for Tokyotech Advanced Research (STAR).

Table 1: Sample parameters: deposition temperature and time, total film thickness, *c*-axis lattice parameter and critical temperatures evaluated from PPMS measurements at $\mu_0 H$ = 0T.

SAMPLE NO.	TEMP. (°C)	DEPOSITION TIME (MIN)	TOTAL THICKNESS (NM)	*C*-AXIS (Å)	T_C (K)		
					90%	*50%*	*10%*
1	650	10	63	8.69	–	–	–
2	860	10	58	8.66	32.6	27.5	23.6
3	860	15	91	8.67	42.8	36.8	30.0

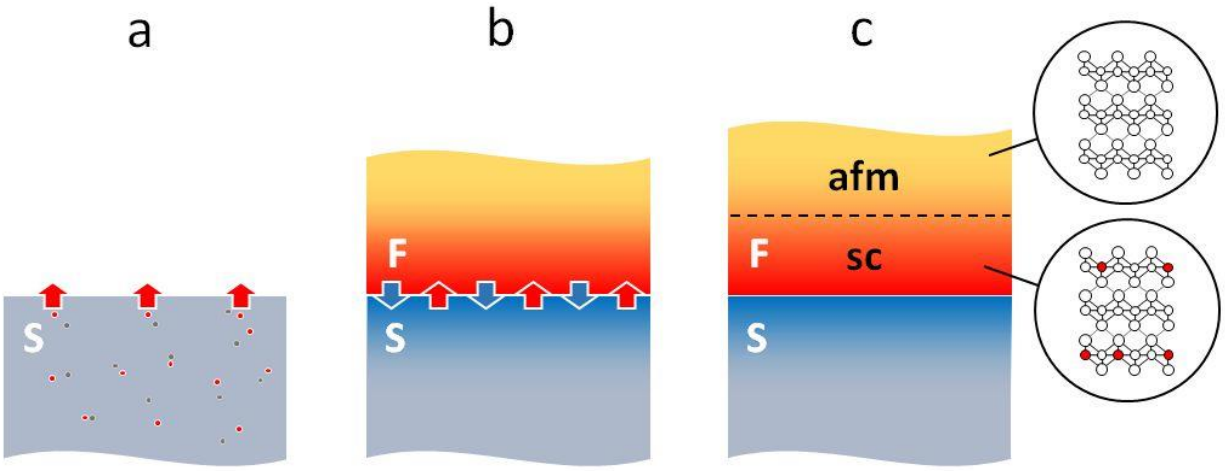

Fig. 1: The layered two-phase hybrid structure of PLD-grown $SmO_{1-x}F_xFeAs$ thin film (F) on CaF_2 substrates (S): a) Heating of the CaF_2 to 860°C rises the mobility of fluorine ions and fluorine vacancies. b) During deposition interdiffusion (arrows) takes place through the F/S interface. The fluorine-content in the film increases with deposition time. c) The resulting thin film can be modeled by a layered two-phase hybrid structure with a superconducting (sc) and a non-superconducting and antiferromagnetic (afm) $SmO_{1-x}F_xFeAs$ phase. Red spheres in the schematic unit cells indicate the variable fluorine content along the thickness.

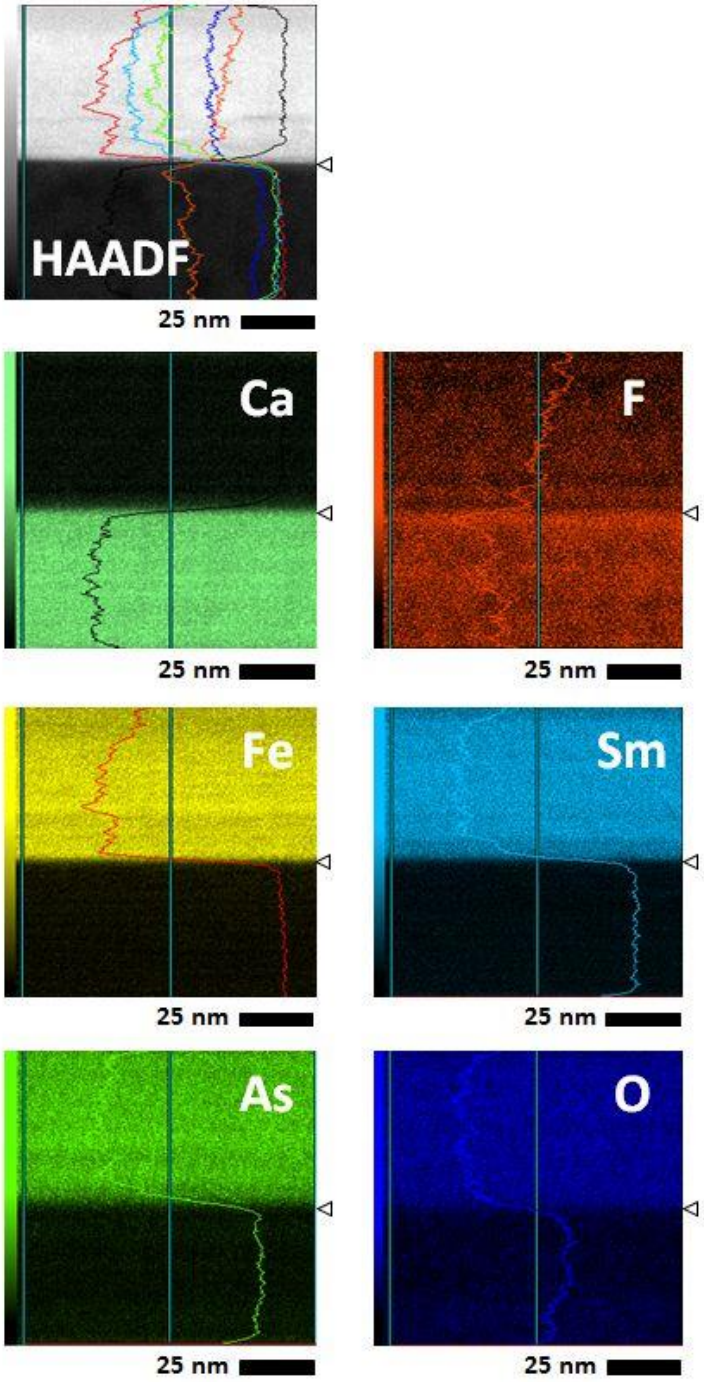

Fig. 2: STEM-EDX mapping for Ca, F, Fe, Sm, As and O in film no. 2. A HAADF image was taken before the mapping. All measured elements display interdiffusion near the F/S interface (location indicated by the arrows).

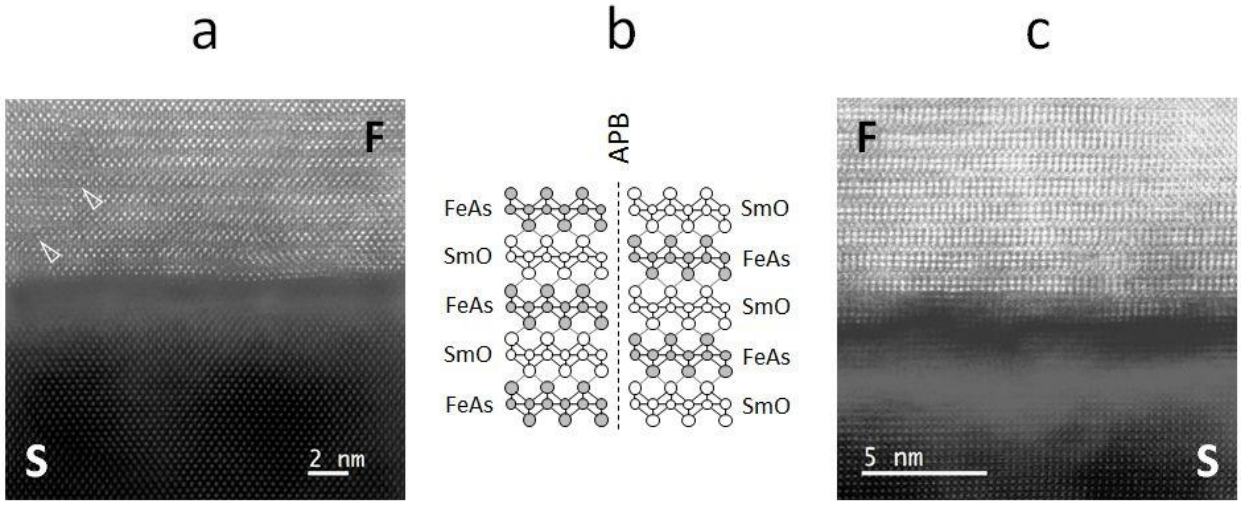

Fig. 3: HAADF-STEM images of the film/substrate (F/S) interfaces of different $SmO_{1-x}F_xFeAs$ thin films grown on CaF_2(001). a) Interface for the film grown at low temperature (film no. 1). The electron beam direction is along CaF_2[110] ‖ SmOFeAs[100]. An APB can be detected, for example, on the left side by a change in contrast where FeAs layers are exchanged by SmO layers (arrows). b) Schematic image of an antiphase-boundary (APB) in SmOFeAs. c) Interface for the film grown at high temperature (film no. 2). The electron beam direction is along CaF_2[100] ‖ SmOFeAs [110].

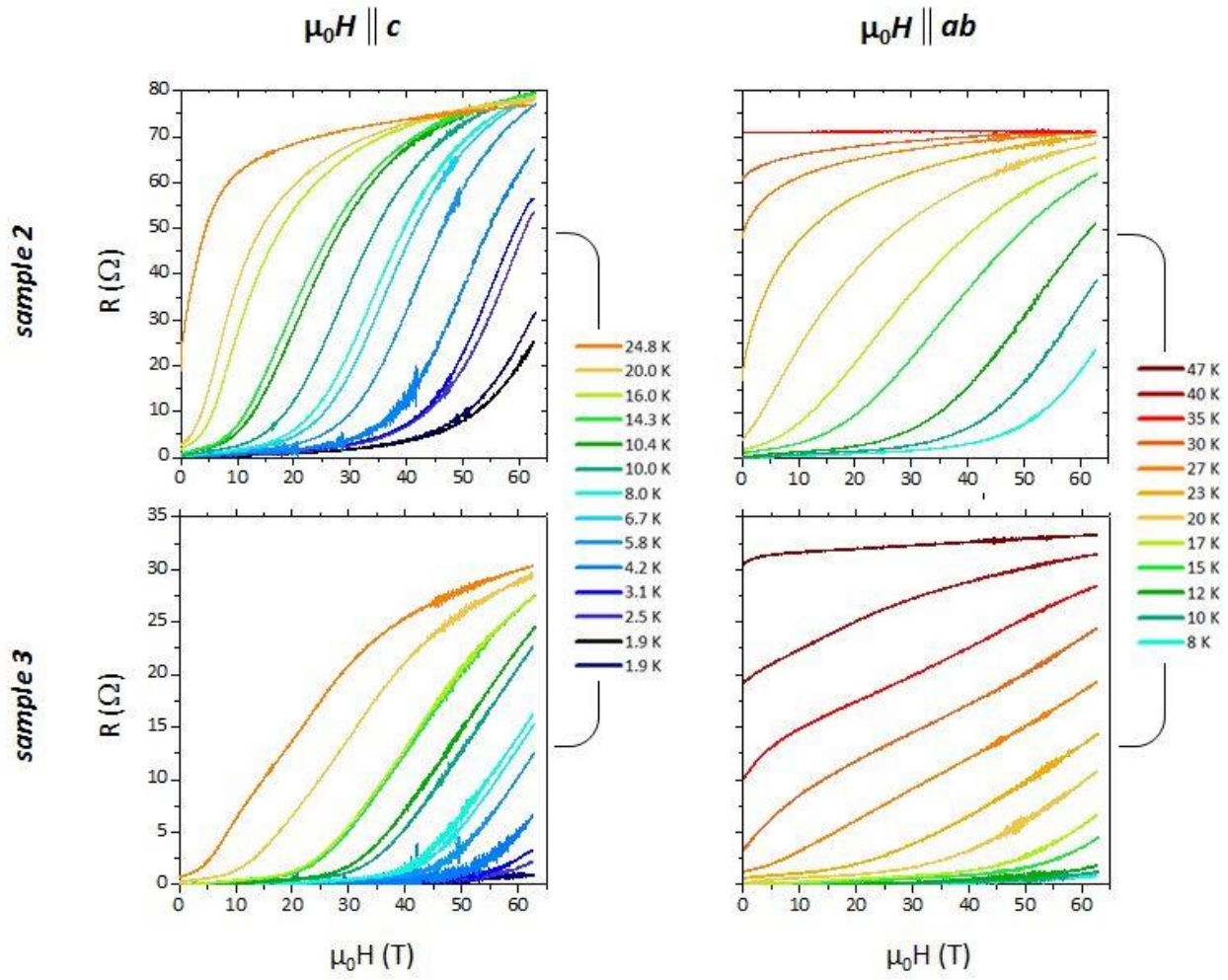

Fig. 4: Magnetic field dependence of the resistance of films nos. 2,3 for two configurations, $\mu_0 H \parallel c$ (left) and $\mu_0 H \parallel ab$ (right) at different temperatures.

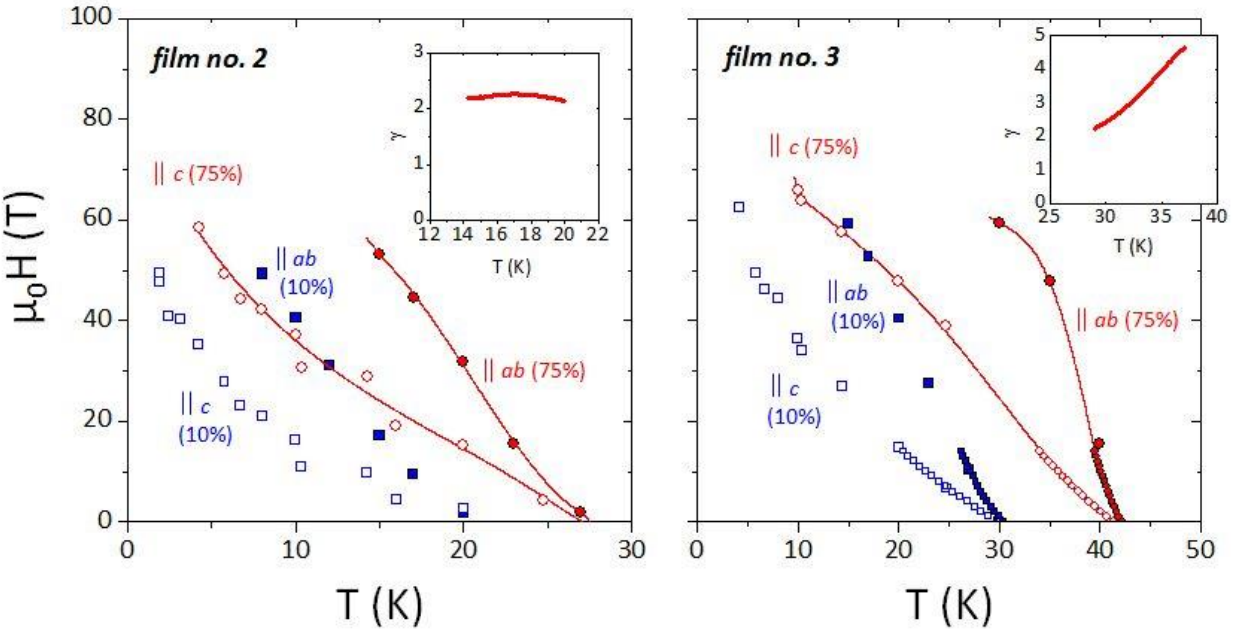

Fig. 5: Upper critical field ‖ *c* (open symbols) and ‖ *ab* (closed symbols) evaluated at 75% of the resistive transition (red). For comparison, the transition was also evaluated at a 10%-criterion (blue). Smaller symbols indicate data evaluated from measurements up to 14 T static magnetic fields (PPMS). Interpolation (red lines) was used for the evaluation of the upper critical field anisotropy, γ (inset).

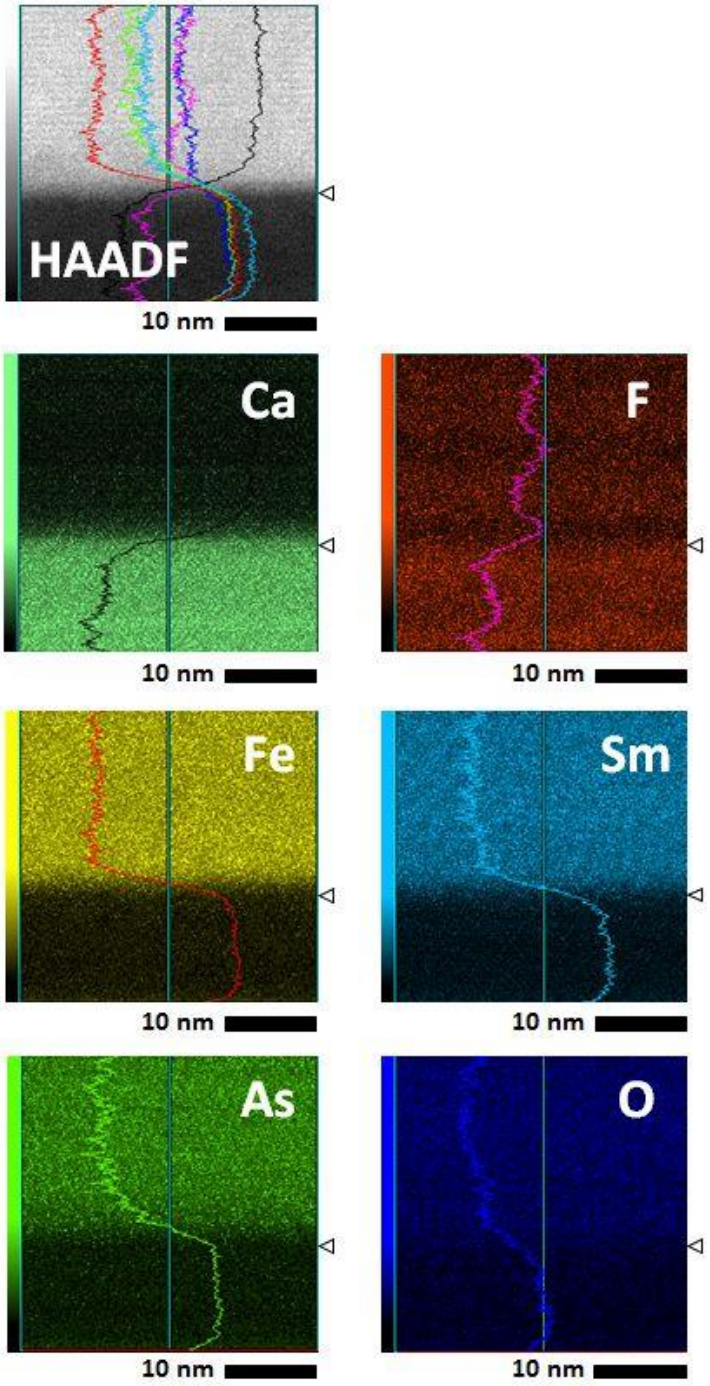

Fig. A1: STEM-EDX mapping for Ca, F, Fe, Sm, As and O in film no. 1. A HAADF image was taken before the measurement.

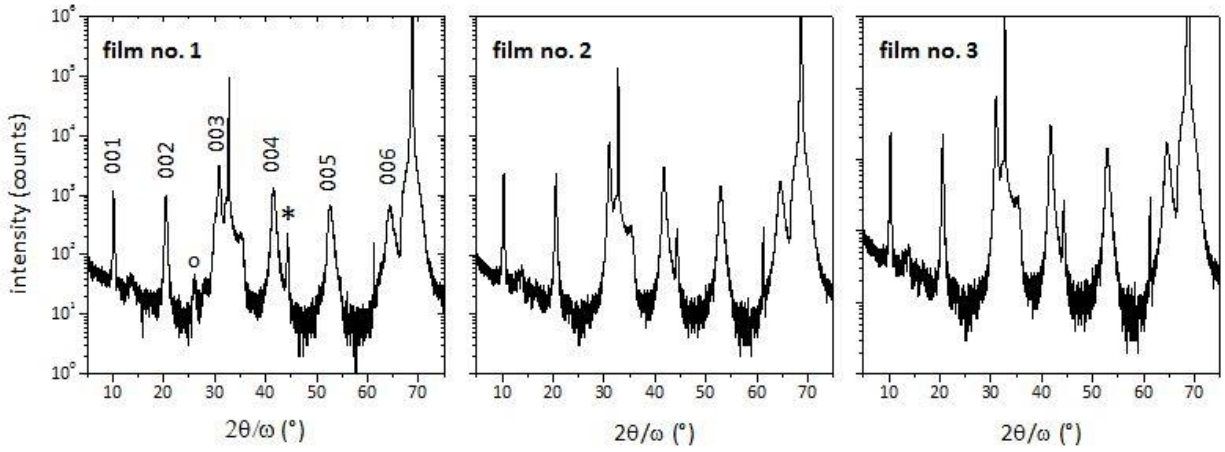

Fig. A2: XRD (Bragg Brentano) for films nos. 1-3.